ADVANCED OPTICAL MATERIALS
www.advopticalmat.de

Noninvasive Injectable Optical Nanosensor-Hydrogel Hybrids Detect Doxorubicin in Living Mice

*Zachary Cohen, Dave J. Alpert, Adam C. Weisel, Amelia Ryan, Arantxa Roach, Syeda Rahman, Pooja V. Gaikwad, Steven B. Nicoll, and Ryan M. Williams**

While the tissue-transparent fluorescence of single-walled carbon nanotubes (SWCNTs) imparts substantial potential for use in non-invasive biosensors, the development of non-invasive systems is yet to be realized. Here, the functionality of a SWCNT-based nanosensor in several injectable SWCNT-hydrogel systems, ultimately finding SWCNT encapsulation in a sulfonated methylcellulose hydrogel optimal for detection of ions, small molecules, and proteins is investigated. It is found that the hydrogel system and nanosensor signal are stable for several weeks in live mice. Then, it is found that this system successfully detects local injections of the chemotherapeutic agent doxorubicin in mice. Future studies to adapt this device for the detection of other analytes in animals and, ultimately, patients are anticipated.

1. Introduction

Single-walled carbon nanotubes (SWCNTs), cylindrical allotropes of carbon, have garnered considerable research interest in recent years for their exceptional mechanical, electrical, and optical properties.[1] In particular, semiconducting SWCNTs exhibit near-infrared fluorescence, making them well-suited to use as transducers in optical biosensors. SWCNTs exhibit large stokes shifts,[2] do not photobleach,[3–4] and fluoresce in the tissue-transparent window. This has enabled implanted SWCNT-based biosensors to retain their fluorescence properties for at least 300 days in vivo,[5] and at depths of 5.5 cm ex vivo.[6] SWCNT-based biosensors have been developed for a variety of analytes, including metal ions,[7–9] nitrous oxide,[10] glucose,[11] chemotherapeutics,[12–13] auxins,[14] insulin.[15] and other hormones,[16–17] neurotransmitters,[18–20] oligonucleotides,[21] riboflavin,[17] fibrinogen,[22] growth factors,[23] amyloid beta,[24] cytokines,[25] lipid accumulation diseases,[26] cardiac biomarkers,[27] cancer biomarkers,[28–29] and more.[30]

To date, several studies have demonstrated SWCNT-based biosensor implants in living animals. SWCNTs can be administered intravenously,[31] which results in SWCNT uptake in the liver Kupffer cells, allowing sensing within those cells.[32] For biosensing in other locations, the majority of studies surgically implanted SWCNTs in either sealed dialysis membranes.[12,21,28] or hydrogels.[5–6,13,16,33–35] Surgical implantation makes biosensing possible at any location, but is by nature an invasive procedure. However, an injectable SWCNT implant, in which SWCNT are encapsulated in an in situ-gelling hydrogel, would enable noninvasive biosensing without necessitating an invasive procedure. One prior study has taken a similar approach in marine organisms, delivering nanotubes dispersed in pre-gelled polymers via trocar.[36] Though innovative, this approach requires larger trochar needles for preformed gels and may be better adapted to the clinic by instead using polymers that gelate in situ post-injection, thereby conforming to nearby tissue. Such injectable hydrogels are already used for cell and drug delivery.[37]

Hydrogels are a diverse and customizable class of materials, many of which have found applications in improving the function and biocompatibility of nanosensors.[38–40] Their chemical properties may be tuned to control their mechanical properties, porosity, biocompatibility, and other properties relevant to injection at numerous physiological locations.[37] They have such diverse applications as platforms for drug and cell delivery, cell recruitment, and as scaffolds for tissue engineering. Their high degree of tunability is important for SWCNT implants in particular, as such a device must facilitate analyte diffusion into the gel while preventing SWCNT diffusion out of the gel. As noted above, several SWCNT-hydrogel hybrid materials have been preformed prior to in vivo implantation.[5–6,13,16,33–35] Such hybrids with SWCNT and other nanomaterials-based sensors allow for more robust, long-term analyte detection as well as potentially improved sensitivity and specificity of the sensor.[38–40]

Other studies have demonstrated impressive performance for surgically implanted hydrogel-encapsulated SWCNTs. Beyond preserving SWCNT fluorescence for 300 days,[5] multiple

Z. Cohen, D. J. Alpert, A. C. Weisel, A. Ryan, A. Roach, S. Rahman, P. V. Gaikwad, S. B. Nicoll, R. M. Williams
The City College of New York
Department of Biomedical Engineering
New York, NY 10031, USA
E-mail: rwilliams4@ccny.cuny.edu
P. V. Gaikwad, R. M. Williams
PhD Program in Chemistry
Graduate Center
The City University of New York
New York, NY 10016, USA

The ORCID identification number(s) for the author(s) of this article can be found under https://doi.org/10.1002/adom.202303324

DOI: 10.1002/adom.202303324

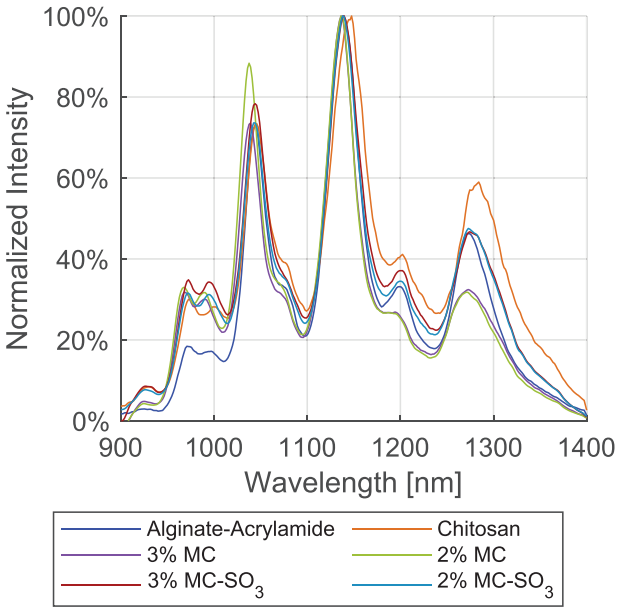

Figure 1. Representative Fluorescence Spectra of the Nanotube Sensor in All Hydrogels Tested.

experiments have shown that hydrogels can reliably sequester SWCNTs without leakage.[35,41] Furthermore, hydrogel-encapsulated SWCNTs have been used to detect such diverse analytes as nitrous oxide,[5,33] progesterone,[16,35] riboflavin,[34–35] ascorbate,[34] and chemotherapeutics.[13] in vivo. These studies commonly employed gels incorporating alginate.[5,33] or poly(ethylene glycol) diacrylate,[13,16,34–35] polymers noted for their biocompatibility.

In this work, we developed a novel injectable hydrogel-encapsulated SWCNT system based on methacrylated methylcellulose (MC).[42] We compared this system to previously-described alginate and chitosan encapsulation systems.[43–44] We found that this novel injectable system responds robustly to a variety of analytes, including magnesium chloride, sodium bicarbonate, the chemotherapeutic doxorubicin (DOX), and bovine serum albumin. We then found that MC-SWCNTs implanted via simple, noninvasive injection showed stable fluorescence for several weeks. Finally, we found that the sensor system responds to DOX in living mice as a model of a clinically relevant analyte.

2. Results and Discussion

The fluorescence of SWCNT-based nanosensors was evaluated in six hydrogels. $(GT)_{15}$-SWCNT fluorescence was detected in all gels tested (**Figure 1**). We used $(GT)_{15}$ ssDNA-SWCNT as a model sensor in all studies as $(GT)_{15}$ ssDNA is known to have a stable interaction with SWCNT through hydrophobic π–π stacking.[47–49] In addition, this model nanosensor has previously demonstrated the ability to respond to a wide array of analytes including magnesium ions.[9] and doxorubicin,[12] though future work will investigate the incorporation of molecularly-specific sensors.

Though the hydrogel is largely hydrophilic, and composed of mostly water, local interactions with charged polymeric materials may dictate the fluorescence emission spectra of fluorescent

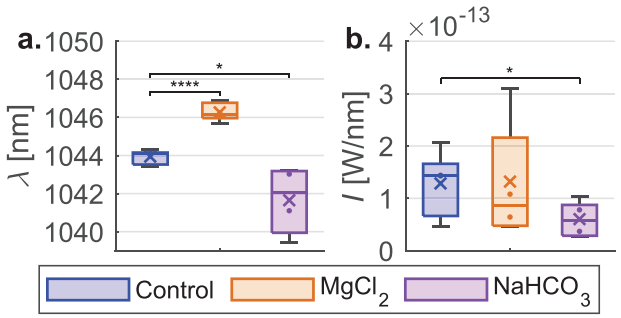

Figure 2. Sensor Response to $MgCl_2$ and $NaHCO_3$ in alginate–acrylamide hydrogels. A) center wavelength and b) intensity. $MgCl_2$ and $NaHCO_3$ induced significant wavelength shifting versus control ($p = 4 \times 10^{-6}$ and .02 respectively), while only $NaHCO_3$ caused a significant intensity change ($p = 0.04$). $n = 6$.

SWCNT.[50] We found that nanotube fluorescence in relatively more positively-charged gels (chitosan) was red-shifted relative to other gels evaluated without positive charges. However, it may be possible that blue-shifted SWCNT in each of the other gel formulations was the result of microaggregation.[51] As intensity was not substantially impacted, however, the former explanation may be the most likely, and we proceeded to study each of the formulations individually.

2.1. Detection of Magnesium Chloride and Sodium Bicarbonate in Alginate–Acrylamide Gels

The first hydrogel tested was a previously described alginate–acrylamide copolymer solution that crosslinks at body temperature.[43] The copolymer is composed primarily of poly(*N*-isopropylacrylamide) grafted to an alginate backbone for extra rigidity. It was selected for these experiments because alginate gels are commonly used in experiments with SWCNTs, while crosslinking at body temperature is appealing for injection.[5,12,33,37] As a naturally-occurring polysaccharide, alginate is highly abundant and biocompatible.[52] It is also known for forming gels relatively easily, especially via the addition of a divalent crosslinker.

The sensing ability of $(GT)_{15}$-SWCNTs in the alginate–acrylamide gel was evaluated using magnesium chloride ($MgCl_2$, 5 M) and sodium bicarbonate ($NaHCO_3$, 1 M) as representative analytes. $MgCl_2$ and $NaHCO_3$ were chosen for this initial response evaluation because their small hydrodynamic radii and high charge were hypothesized to better facilitate diffusion and detection. $MgCl_2$ was of particular interest as previous studies have demonstrated good detection of divalent cations by SWCNTs through an induced rearrangement of the ssDNA structure on the surface of the nanotube.[7–9] Sodium bicarbonate, however, is suspected to undergo reduction when contacting the surface of the nanotube. After SWCNT-containing alginate–acrylamide gels were incubated with the analytes for one hour at body temperature, $NaHCO_3$ was found to cause partial quenching (intensity decreased by 53 ± 54% versus control) and blue-shifting (−2.3 ± 1.8 nm). $MgCl_2$ only caused shifting (2.3 ± 0.6 nm, **Figure 2**), though this shift was more consistent than that induced by $NaHCO_3$.

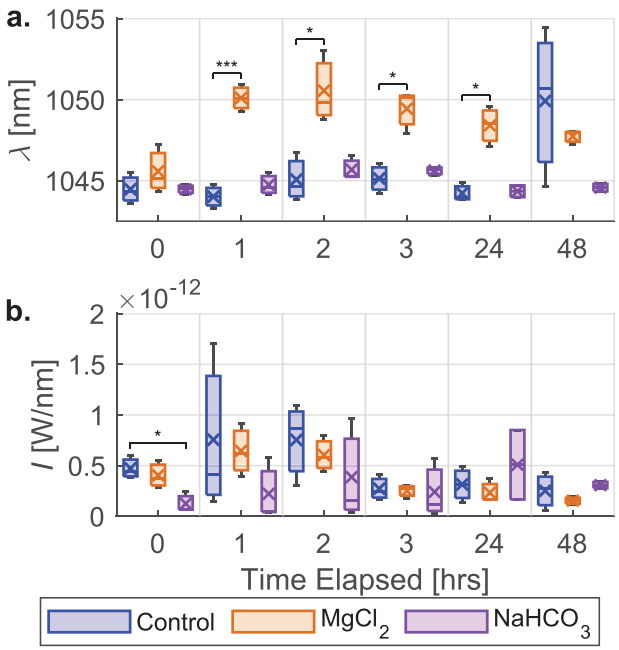

Figure 3. Sensor Response to $MgCl_2$ and $NaHCO_3$ in a chitosan-based hydrogel. A) center wavelength and b) intensity. $NaHCO_3$ did not cause shifting at any timepoint; $MgCl_2$ induced significant shifting on hours 1, 2, 3, and 24 ($p = 8 \times 10^{-4}$, 03, 01, and .02 respectively). No significant differences were observed in intensities. $n = 3$.

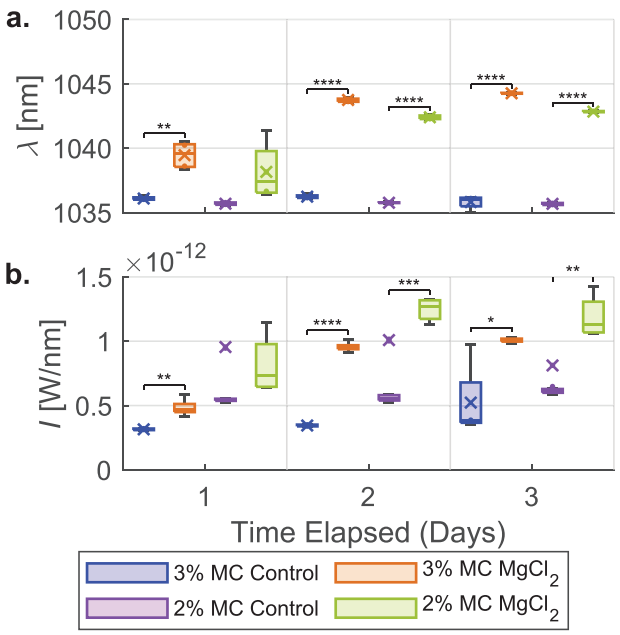

Figure 4. Sensor Response to $MgCl_2$ in MC-based hydrogels. A) center wavelength and b) intensity. *p*-values for 3% MC shifts on days one through three were .001, 4×10^{-10}, and 6×10^{-5} respectively; *p*-values for 2% MC on days two and three were 2×10^{-6} and 2×10^{-12} respectively. *p*-values for 3% MC intensity changes on days one through three were .004, 9×10^{-7}, and .048 respectively; *p*-values for 2% MC on days two and three were 3×10^{-4} and .006 respectively. $n = 4$–5.

2.2. Detection of $MgCl_2$ and $NaHCO_3$ in Chitosan Gels

We then investigated sensor encapsulation in a chitosan gel, also known to crosslink at body temperature, whose mechanical properties were previously shown to improve upon the incorporation of graphene oxide.[44] Similar to alginate, chitosan was an appealing polymer because of its abundance and biocompatibility.[52] The sensing ability of $(GT)_{15}$-SWCNTs in the chitosan gel was again evaluated using $MgCl_2$ (5 M) and $NaHCO_3$ (1 M) as model analytes (**Figure 3**). While neither caused an intensity-based response, $MgCl_2$ induced red-shifting (6.1 ± 1.1 nm) which plateaued after an hour and then decreased by a third (to 4.2 ± 1.4) nm after the first day. We found minimal response to $NaHCO_3$, likely because the gel is itself basic.

2.3. Detection of $MgCl_2$ and $NaHCO_3$ in Methylcellulose Gels

While both the chitosan and alginate–acrylamide gels gave acceptable results for model analyte detection, they are known to be less mechanically robust than desirable for long-term implantation.[43–44] This prompted us to investigate a gel based on methacrylated methylcellulose (MC) with demonstrated biocompatibility and mechanical properties facilitating long-term in vivo stability.[42] This particular gel was originally investigated for tissue engineering applications, and therefore is already well-suited to clinical translation. Additionally, cellulose is the most naturally abundant polysaccharide and is therefore easy to source.[52]

MC gels were initially tested at polymer concentrations of 2% and 3%. While 3% MC gels were previously shown to have optimal mechanical properties for implantation as an adipose tissue mimic, 2% MC gels were speculated to better facilitate analyte diffusion because of their higher porosity.[42] Though neither MC-SWCNT formulation responded to $MgCl_2$ (5 M) by the first day, large redshifts were observed two days into the experiment (**Figure 4**, 7.5 ± 0.2 nm and 6.6 ± 0.2 nm for 3% and 2% gels respectively). While 2% MC was not found to perform better than 3% MC for $MgCl_2$ detection, a similar experiment found that $NaHCO_3$ (1 M) only elicited a response from the 2% system, inducing red shifting two days after exposure (**Figure 5**, 1.6 ± 0.5 nm). It is notable that variability in the detection of $MgCl_2$ with the MC system was generally lower than in previous studies, which may have resulted from general homogeneity in gel preparation or a more stable interaction of SWCNT with this polymer.

In comparison to the chitosan and alginate–acrylamide gel systems for the detection of $MgCl_2$, it is notable that the response occurs over a longer timeframe of hours compared to one day. This difference may be due to the interaction of this analyte itself with each gel, or possibly unreacted redox initiators in the MC gel. We also note that detection in the prior two systems diminished over time, likely due to increased dehydration and heterogeneity when compared to the MC-SWCNT system. Finally, our in vitro testing conditions in a static cuvette format are not indicative of conditions in vivo that would include external mechanical and fluidic forces.

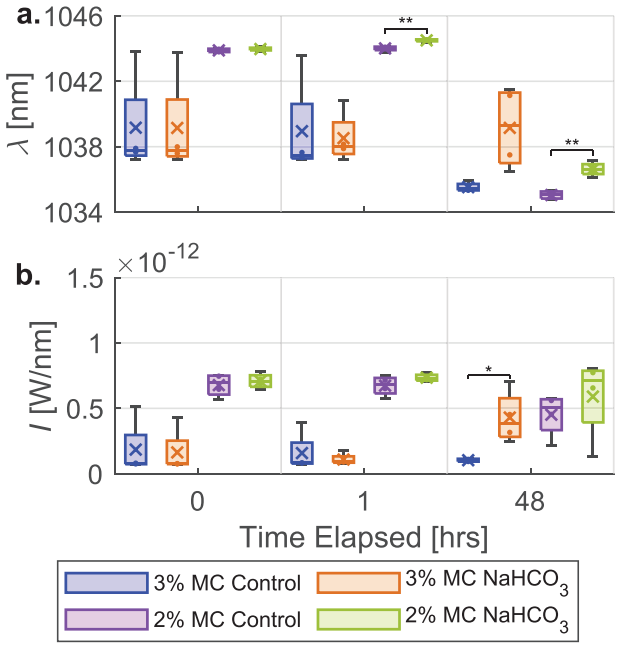

Figure 5. Sensor Response to $NaHCO_3$ in MC-based hydrogels. A) center wavelength and b) intensity. The 2% sensor gel exhibited a slight but significant shift at hours one and 48 ($p = 0.004$ and .001 respectively), whereas the 3% sensor gel system only showed a significant intensity-based response on the second day ($p = 0.047$). $n = 3$–4.

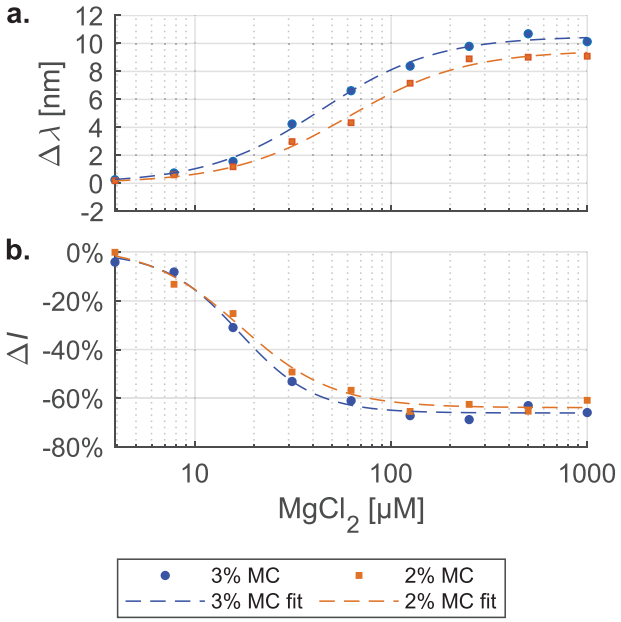

Figure 6. $MgCl_2$ Quantification in MC Based Hydrogels. A) shift and b) intensity change. Fits use the Hill model; $R^2 \geq 0.99$ for all fits. Shift-derived K_D values are 44.1 and 60.3 μM for 3% and 2% gels respectively; intensity change-derived K_D values are 16.9 and 17.1 μM for 3% and 2% gels respectively.

2.4. $MgCl_2$ Quantification in Methylcellulose Gels

Because the MC-SWCNT system demonstrated the most substantial responses and has the most desirable mechanical properties, we further explored this system to evaluate the breadth of MC's potential as an in vivo sensor delivery platform. To evaluate the system's capacity for analyte quantification across a range of concentrations, MC-SWCNT samples were topped with $MgCl_2$ from 4 to 1000 μM. Concentration-dependent shift- and intensity-based responses were observed after two days (**Figure 6**) and fit to a Hill model. Interestingly, the intensity-based response was found to have higher sensitivity, with a fit-derived K_D of about 20 μM, compared to about 50 μM for the shift response. The decoupled nature of shifting and intensity responses may allow for analyte quantification across a broader range of concentrations than would otherwise be possible.[53]

2.5. Detection of $MgCl_2$ and Bovine Serum Albumin in Sulfonated Methylcellulose Gels

To potentially increase the response rate while maintaining the MC-SWCNT system's mechanical properties, sulfonated versions were also investigated. As MC gels are largely hydrophobic, it was hypothesized that increasing polymer hydrophilicity by charge functionalization would better facilitate the diffusion of salts and proteins. Sulfonate groups were added to the MC polymers by replacing some of the methacrylate groups prior to gelation. This was accomplished by adapting a previously described modification of our gel preparation procedure.[54] SWCNTs encapsulated in sulfonated 3% MC exhibited fluorescence across the entire 149-day duration of a stability assessment experiment (Figure S2, Supporting Information). Separately, we performed an additional study to evaluate whether SWCNT leached from the gel over a one-week timeframe. Five 1 mL gels were cast in cuvettes, with NIR fluorescence obtained 30 min after casting. The gels were then submerged in a 30 mL volume of PBS for one week and spectra were obtained daily. In this study, we found that hydration of the gel brightened the SWCNT spectra, and we found no reduction in fluorescence intensity from Day 1 to 7 (Figure S3A, Supporting Information). To further evaluate whether any SWCNT leached from the gel into the PBS, we obtained fluorescence spectra at each day, finding no signature of SWCNT emission (Figure S3B, Supporting Information). To ensure this result, we concentrated the 30 mL volume down to 1 mL at Day 7, again finding no signature of SWCNT Emission. Following gelation of the 3% sulfonated methylcellulose formulation with encapsulated SWCNTs, we found that its viscoelastic properties were maintained in comparison to controls with minor, but non-significant reductions in elasticity modulus, loss modulus, and gelation time (Figure S4, Supporting Information).

Concentrations having 2% and 3% of the sulfonated methylcellulose (MC-SO_3) gel with $(GT)_{15}$-SWCNTs were evaluated for their response to $MgCl_2$ (5 M) and bovine serum albumin (BSA, 600 μM). BSA was introduced as a representative large molecular weight globular protein given prior studies demonstrating a hydrophobic adsorption of BSA protein to the surface of the nanotube.[55] It should be noted that non-invasive sensing of albumin has particularly important clinical implications in liver, renal, and cardiovascular disorders.[56] Indeed, a SWNCT-based

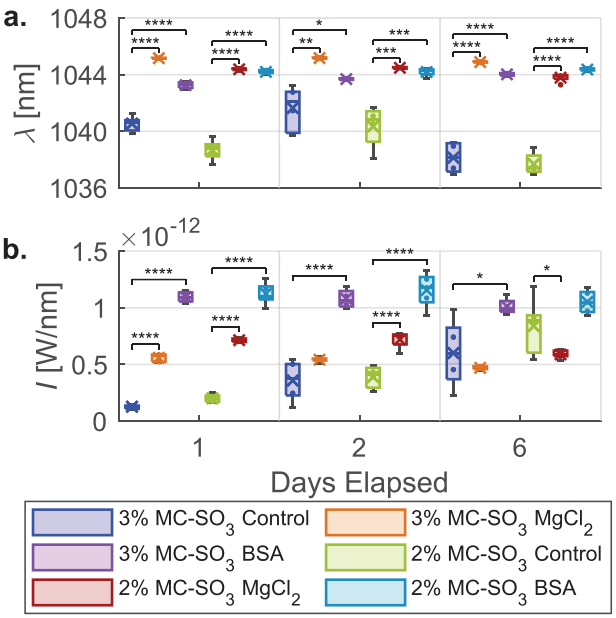

Figure 7. Sensor Response to $MgCl_2$ and BSA in Sulfonated MC Hydrogels. A) center wavelength and b) intensity. Significant wavelength ($p < 0.0001$, Table S1, Supporting Information) differences were observed for all groups on days 1 and 6; significant intensity differences ($p < 0.0001$, Table S2, Supporting Information) were observed for all groups on days 1 and 2 (except for $MgCl_2$ on day 2 in 2% MC-SO_3). $n \geq 4$.

nanosensor paint has previously been reported for the preclinical detection of microalbuminuria.[57] Both the sulfonated systems were found to have significant shift- and intensity-based responses to $MgCl_2$ or BSA one day after incubation, an improved detection speed compared to the non-sulfonated devices (**Figure 7**). At this timepoint, the 3% gel-encapsulated SWCNTs responded to BSA with a shift and intensity change of +2.7 ± 0.6 and +660 ± 42% respectively; for the 2% system wavelength and intensity responses of +5.5 ± 0.7 and +360 ± 50% were observed. While wavelength shifts were maintained throughout the experiment, intensity differences moderated between days 2 and 6, largely due to increases in control intensity rather than diminution of analyte response. Following the success of these initial investigations into MC-SO_3, an experiment was conducted to determine the effect of gel sulfonation on analyte detection. These experiments established that, as hypothesized, MC sulfonation improved BSA detection speed (Figure S5, Supporting Information). Sulfonation was also shown to increase BSA response magnitude.

BSA diffusion into MC gels was confirmed by a BCA assay (Figure S6, Supporting Information). Analyte-containing topping solutions were removed and replaced with a solution of cellulose. Protein quantification was then performed on the degraded gels to determine the amount of BSA present, finding that gels exposed to BSA contained 130–250 µM of the protein, and that there were no clear differences in diffusion between the 2% and 3% gels.

We then evaluated the ability of the 3% MC-SO_3-SWCNT system to maintain its BSA response over a two-week period. The 2% MC formulation was not used because sulfonation had a greater impact on response speed and the 3% concentration better approximates tissue. Significant wavelength- and intensity-based responses were observed across the entire experiment duration (Figure S7, Supporting Information). We found that the wavelength-based response diminished across the experiment duration (from +8.9 ± 0.5 nm to +2.9 ± 1 nm), whereas the intensity response plateaued after three days (at +62% ± 10% of the control's intensity). While the wavelength-based response can largely be attributed to red-shifting of the experimental group, the intensity-based response derives from intensity changes in the control group (Figure S8, Supporting Information). It is possible that this increased intensity from Day 1 to Day 2 is due to increased time for interaction of SWCNTs with electron-donating species, such as unreacted vinyl groups in the methacrylated-MC polymer. This is consistent with the literature, which has previously shown that electron donors increase fluorescence intensity.[58]

2.6. Quantification of BSA and Doxorubicin in Sulfonated Methylcellulose Gels

Concentration-response curves were obtained in gel and solution to evaluate the effect of 3% MC-SO_3 encapsulation on $(GT)_{15}$-SWCNT response dynamics at 37 °C. Responses were measured at analyte concentrations from 10 nM to 10 mM. These experiments were executed using a high-throughput 96-well plate format, enabled by a custom-built near-IR plate-reader spectrophotometer. Responses were fit to a logistic trend (Equation S2, Supporting Information). Here, we again investigated responses to albumin while separately introducing a new analyte, doxorubicin (DOX). DOX is a small molecule anthracycline chemotherapeutic used as a front-line therapy in several cancers.[21] Our previous studies demonstrated SWCNT-based fluorescent sensors implanted within a dialysis membrane for DOX pharmacokinetic monitoring in mice.[21] Those studies hypothesized that the detection of DOX with $(GT)_{15}$-SWCNT occurred through the binding of the hydrophobic small molecule to the surface of the nanotube.

Whereas 3% MC-SO_3 encapsulation increased BSA sensitivity (**Figure 8**; Figures S9 and S10, Supporting Information) and response magnitude versus solution conditions, it also decreased DOX sensitivity (**Figure 9**; Figures S11 and S12, Supporting Information). For BSA, the shift-derived K_D decreased by one to two orders of magnitude for every chirality except (8,7) (e.g., 920 to 16.7 µM for the (7,5) chirality, Table S4, Supporting Information). Interestingly, intensity change-derived K_D values did not change appreciably (Table S5, Supporting Information). The lower limits of detection (LOD) for BSA were generally an order of magnitude lower in the gel versus in solution for wavelength-based measurements, however they were largely similar for intensity-based measurements (Tables S4 and S5, Supporting Information). For either intensity or wavelength measurements, the lowest-calculated LOD was ≈1 µM. Prior studies demonstrated a SWCNT-based optical sensor for albumin, with the goal of detecting microalbuminuria, had an LOD of ≈100 nM in solution and 1 µM when embedded in an acrylic paint.[57] That sensor was designed by screening various helical polymers when wrapped around SWCNT for their albumin interaction instead of ssDNA, though the paint-based LOD of

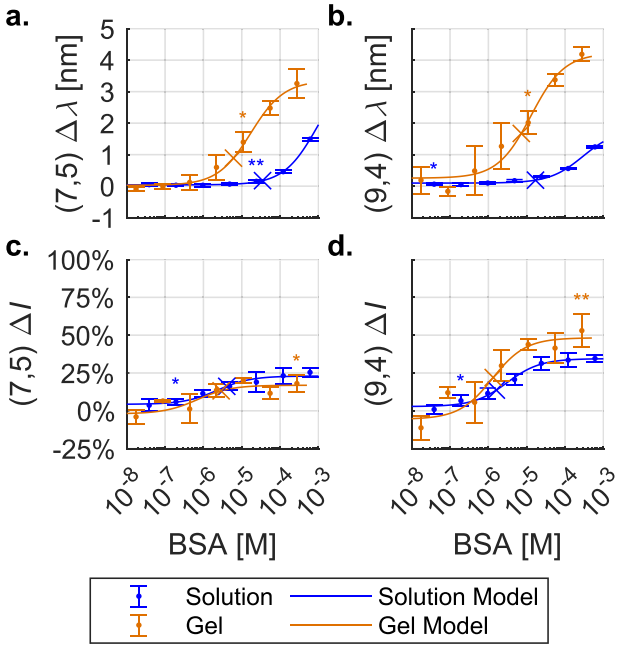

Figure 8. Quantification of BSA in 3% MC-SO_3 Hydrogels and Solution. Shifts of a) (7,5) and b) (9,4) chiralities. Intensity changes of c) (7,5) and d) (9,4) chiralities. Data were fit to a logistic model (Equation S2, Supporting Information); fit parameters/quality were recorded in Supporting Information (Tables S4 and S5). Crosses represent lower limits of detection (Tables S4-5), calculated as the analyte concentration producing a signal equal to three times the noise (Equation S3, Supporting Information). Significance markers are only shown for the lowest BSA concentration to produce a statistically significant difference from the control ($p < 0.05$). $n = 3$ samples per concentration.

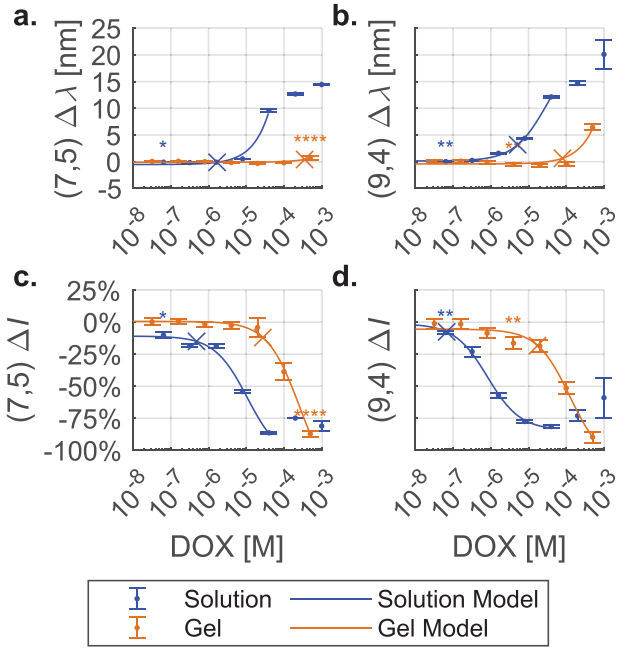

Figure 9. Quantification of Doxorubicin in 3% MC-SO_3 Hydrogels and Solution. Shifts of a) (7,5) and b) (9,4) chiralities. Intensity changes of c) (7,5) and d) (9,4) chiralities. Data were fit to a logistic model (Equation S2, Supporting Information); fit parameters/quality were recorded in Supporting Information (Tables S6-,S7, Supporting Information). Crosses represent lower limits of detection (Tables S6,S7, Supporting Information), calculated as the analyte concentration producing a signal equal to three times the noise (Equation S3, Supporting Information). Significance markers are only shown for the lowest DOX concentration to produce a statistically significant difference from the control ($p < 0.05$). $n = 3$ samples per concentration. For solution data, the model was not extended to concentrations that disobeyed the trend because of DOX aggregation. These concentrations were also excluded from detection limit calculations.

≈1 µM demonstrated utility in detecting albuminuria in patient samples.[57]

In contrast, gel encapsulation increased the intensity change and wavelength-derived DOX K_D by one to two orders of magnitude (e.g., 10.7 to 134 µM for the (7,5) chirality, Tables S6 and S7, Supporting Information). However, the MC-SO_3 system better fit the expected trend across the tested concentration range, likely due to DOX aggregation at 10 µM in 1X PBS.[59] Similarly, the LOD fox DOX in solution was one to two orders of magnitude lower than that in the gel. Intensity-based LODs for DOX ranged from 8–42 µM in the gel, whereas they were as low as 68 nM in the solution (Tables S6 and S7, Supporting Information). Our prior work used the same $(GT)_{15}$-SWCNT sensor construct to detect doxorubicin as low as 500 nM across several different chiralities in solution.[12] Prior clinical studies demonstrated that DOX may appear in patient blood in concentrations up to 920 nM, therefore additional studies to further improve the LOD in the gel, more inline with solution-based measurements, are necessary for clinical development.[60]

For both analytes, the response curve goodness-of-fit was decreased after gel encapsulation, likely because of variance in gel volumes expelled by the dual-barrel syringe (Tables S4–S6, Supporting Information). In the case of BSA, this increased variance is partially offset by an increased shift magnitude, leading to a higher signal-to-noise ratio. Response times also increased; whereas the maximum responses were achieved by the first hour in solution, the maximum BSA and DOX responses were observed after 24 and 48 h respectively.

2.7. Doxorubicin Detection in Vivo

Following in vitro validation of this system, we sought to detect the small molecule chemotherapeutic doxorubicin in live animals. The methylcellulose pre-polymer solution is injected as a liquid and forms stable hydrogels at the target location via a dual mechanism. The biopolymer undergoes thermal gelation at body temperature due to hydrophobic interactions between methoxy groups, and forms covalent crosslinks by redox-initiated, free-radical polymerization between methacrylate groups substituted along the cellulosic backbone. Formulations incorporating these modified methylcellulose macromers are effective for soft tissue bulking applications[42] and to exhibit excellent biocompatibility and stability when injected subcutaneously in rodents.[61]

First, we injected a mouse with MC-SO_3-encapsulated SWCNTs to evaluate the stability of the device in vivo. Clear near-infrared fluorescence emanating from gel-encapsulated SWCNTs was observed on each day investigated, up to two months post-injection. Minimal variations in emission spectra were noted upon excitation at 655 and 730 nm (**Figure 10**). Given that

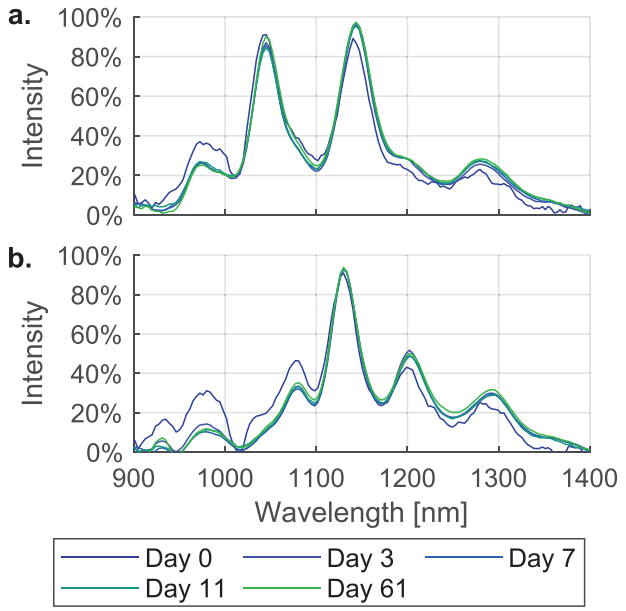

Figure 10. Fluorescence Spectra from $(GT)_{15}$-SWCNT Encapsulated in 3% MC-SO_3 Hydrogels Subcutaneously Injected Across 61 Days. a) 655 nm excitation b) 730 nm excitation.

the fluorescent spectra were relatively similar and stable over the course of 61 days, we concluded that there was minimal if any leakage of the sensor from the gel. If leakage had occurred, it would have been exceedingly difficult to obtain repeatable bright fluorescent spectra at Days 3, 7, 11, and 61 post-injection. Further, the spectra of any SWCNT outside of the gels would be shifted if free within the subcutaneous space instead of the gel. However, given that the spectra were consistent over time after excitation with either laser source, we conclude that the gel implant was stable and with very little leakage.

To evaluate the function of the MC-SO_3-SWCNT formulation in vivo, it was injected into six mice. After the implants were allowed to crosslink (≈15 min), the mice were anesthetized with isoflurane, and baseline spectra were acquired using an IRina NIR-II spectral probe with 655 and 730 nm excitation lasers coupled to an InGaAs detector. Mice were then subcutaneously dosed with DOX or 1X PBS as control at four sites around the implant location ($n = 3$). Fluorescence spectra were again acquired immediately, 10 min, 4, 24, and 48 h post-dosing.

Analyses of these spectra showed that the implants exhibited a shifting-based response to DOX in vivo (**Figure 11**). DOX caused the (7,6) and (9,4) chiralities to shift (experimental minus control) by 1.3 ± 0.5 and 1.2 ± 0.6 nm respectively by the 4 h timepoint (Figure 11), whereas the relatively dim (8,6) chirality only showed a significant response after 48 h (Figures S13 and S14, Supporting Information). Shifts at the 48 h timepoint for the (7,6), (9,4), and (8,6) chiralities were, 1.7 ± 0.5, 0.6 ± 0.2, and 1.1 ± 0.3 nm respectively. The (7,5) chirality was also bright enough to be accurately fit, but exhibited no response (Figures S13 and S14, Supporting Information).

While it was not possible to observe quenching because of high variation in both experimental and control group intensities (attributable to differences in sensor positioning across measurements), DOX did cause a ratiometric intensity response (**Figure 12**). In the experimental group, the (9,4) chirality got dimmer relative to the (7,6); the same effect was not observed in the control group.

While we have previously demonstrated in vivo DOX detection by $(GT)_{15}$-SWCNTs implanted in dialysis membranes, we believe this novel approach utilizing an injectable hydrogel has better potential for clinical translation.[12] It is likely that such an injectable, in situ stabilizing nanosensor formulation has substantially stronger potential due to its lower invasiveness.

3. Conclusion

We found that 3% MC-SO_3 is a functional platform for SWCNT-based biosensor encapsulation, demonstrating the potential of injectable hydrogels as a non-invasive means of implanting SWCNT biosensors. Beyond confirming that a salt ($MgCl_2$) and a representative small-molecule drug (DOX) diffuse through the polymer matrix, we also observed that BSA, a 66.5 kDa protein, was able to permeate the gel and interact with SWCNTs. This confirms that the pore size of 3% MC-SO_3 is not an obstacle to large biomarker diffusion. Our prior studies found that a 3% MC gel of similar composition had an empirical mesh size of 50 nm,[42] whereas the maximum dimension of BSA is 8.3 nm.[62] Although modifications such as sulfonation may modify the mesh size, it is unlikely to limit the diffusion of BSA. These experiments have also demonstrated that relatively precise analyte quantification is possible with this method of SWCNT encapsulation and delivery; logistic models of $(GT)_{15}$-SWCNT fluorescence response as a function of analyte concentration showed R^2 values as high as 0.99. For detection of the model globular protein analyte BSA, both response sensitivity and magnitude were increased in MC-SO_3 compared to the solution. The system also exhibits promising stability and functionality in vivo; implanted in mice, the sensors were shown to fluoresce for at least 61 days, and to discriminate mice injected with DOX from those injected with PBS as a control. We anticipate that further studies will evaluate long-term compatibility for clinical use of this hydrogel-nanosensor system while incorporating molecularly-specific sensors beyond the generally applicable $(GT)_{15}$-SWCNT.

4. Experimental Section

Sensor Preparation: $(GT)_{15}$-SWCNTs were prepared as previously described.[28,45] Briefly, in a 1.5 mL microcentrifuge tube, ≈0.5 mg HiPCO SWCNTs (NanoIntegris, Boisbriand, Quebec, Canada) and $(GT)_{15}$ single-stranded DNA (10 g L^{-1}, Integrated DNA Technologies, Coralville, IA, USA) suspended in 1X PBS (phosphate-buffered saline, Sigma–Aldrich, St. Louis, MO, USA) were added to a final oligonucleotide:SWCNT mass ratio of 2:1. 1X PBS was added to bring the final volume to 500 µL. To achieve aqueous dispersion of SWCNTs by $(GT)_{15}$, the solution was sonicated (1 h, 40% amplitude) in an ice bath by a VCX 750 (Sonics & Materials, Inc., Newtown, CT, USA) fitted with a 2 mm stepped-microtip. The suspension was then ultracentrifuged (58 000 × g, 1 h, 4 °C) in an Optima MAX-XP (Beckman Coulter, Indianapolis, IN, USA) to separate residual catalyst, amorphous carbon, and any partially suspended SWCNTs from the $(GT)_{15}$-SWCNTs. The top 75% of the solution was stored at 4 °C until further use.

Prior to an experiment, excess $(GT)_{15}$ was removed by filtration. An aliquot (100–375 µL) of the $(GT)_{15}$-SWCNT solution was loaded into a

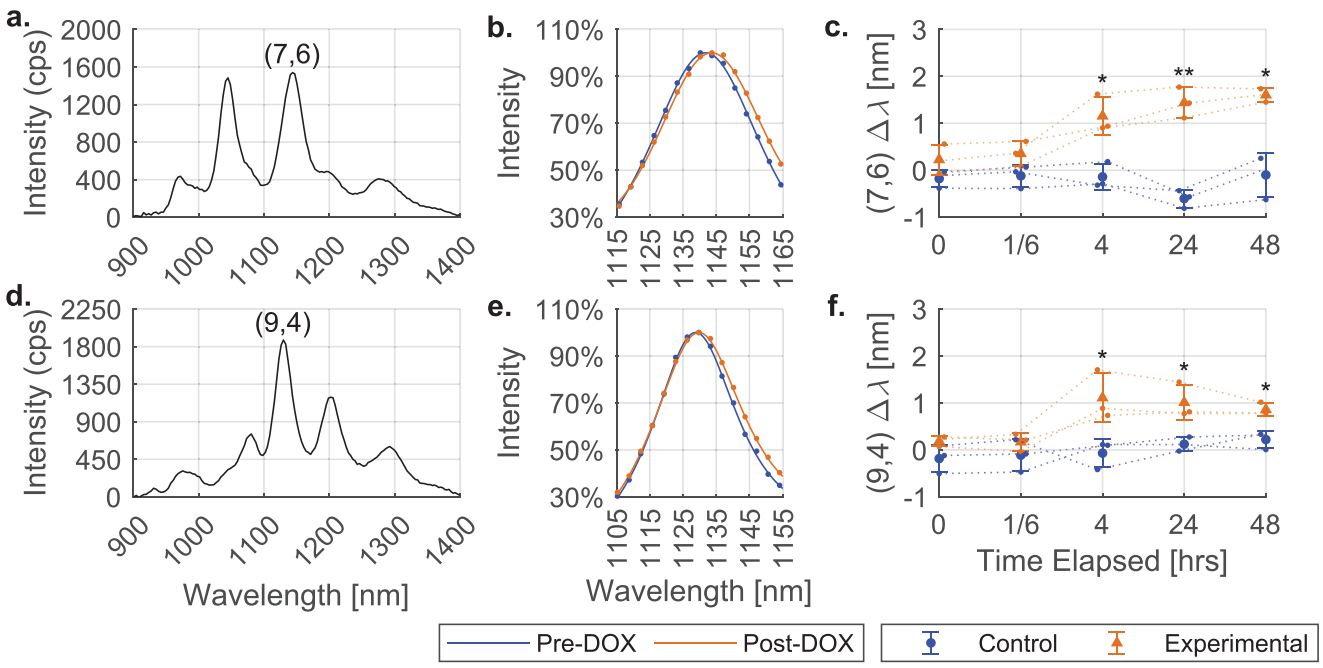

Figure 11. DOX Wavelength Response of Sensor Implants in Vivo. Representative autofluorescence-subtracted spectra of implants in vivo with a) 655 nm excitation and d) 730 nm excitation. Fluorescence peaks (data as dots, models as lines) from the same mouse just before and two days after DOX administration of b) (7,6) and e) (9,4) chiralities. Shifting over time of implants in control and experimental groups for c) (7,6) and d) (9,4) chiralities. $n = 3$. Error bars represent standard deviations. The significance of experimental shift versus control is reported in Table S7 (Supporting Information).

100 kDa molecular weight cutoff filter (Millipore Sigma, St. Louis, MO, USA) and centrifuged (14 000 RPM, 15 min, 4 °C) in a Sorvall ST8R centrifuge (Thermo Fisher Scientific, Waltham, MA, USA). The filtrate was discarded, the contents of the filter were resuspended in 1X PBS (500 µL), and centrifugally filtered again. $(GT)_{15}$-SWCNTs remaining in the filter were resuspended in 1X PBS (100–200 µL).

The resultant solution was characterized by absorbance spectroscopy as previously described.[28,45] Briefly, a visible absorbance spectrum was acquired from the $(GT)_{15}$-SWCNTs using a V-730 UV–Vis spectrophotometer (JASCO, Easton, MD, USA). Concentration was determined using an empirically derived extinction coefficient of 0.036 L mg^{-1} cm^{-1} for the absorption minimum at ~ 630 nm.[27]

Fluorescence Spectrum Acquisition & Analysis: Final $(GT)_{15}$-SWCNT concentrations were 1 mg L^{-1} across all experiments. For experiments using the NS MiniTracer (Applied NanoFluorescence, TX, USA), samples were excited using a 50 mW 638 nm laser with 1–3 s exposure time. For experiments using the ClaIR IR plate reader (Photon Etc., Montreal, Quebec, Canada), samples were excited at 655 and 730 nm (sequentially) for 0.5 s at 1.75 W. For in vivo experiments using the IRina in vivo NIR II spectral probe (Photon Etc.), spectra were acquired with de-focused 1 W laser excitation at 655 and 730 nm (sequentially), 1 s exposures, 1 × 2 binning, manual dark subtraction, and manual autofluorescence subtraction. Autofluorescence was modeled as exponential decay.

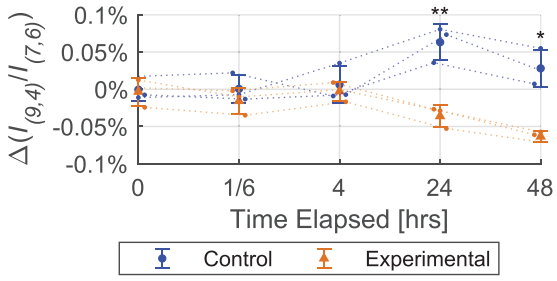

Figure 12. DOX Ratiometric Response of Sensor Implants in Vivo. Percent change in ratio of (9,4) fluorescence intensity to (7,6) fluorescence intensity. In the experimental group, the (9,4) chirality got dimmer relative to the (7,6) chirality. This relative dimming was not observed for the control group. $p = .007$ and .02 at hours 24 and 48 respectively.

Fluorescence peaks were assigned to chiralities based on optical characterization in the literature.[46] To determine the center wavelength and intensity of the (7,5) E_{11} peak, the 24 points closest to the emission maximum around 1035–1045 nm were fit to a pseudo–Voigt model (Figure S1 and Equation S1, Supporting Information) using custom MATLAB code. Fits of other chiralities were performed similarly, using consistent numbers of points for each peak (14 points for less prominent peaks, 28 points for broader peaks). Fits of binned spectra were performed using half as many data points. All analyses presented used fits deemed to be of sufficiently high quality ($R^2 \geq 0.9$).

Magnesium Chloride ($MgCl_2$) and Sodium Bicarbonate ($NaHCO_3$) Detection in Alginate–Acrylamide Gels: $(GT)_{15}$-SWCNT-containing (1.0 mg L^{-1}) alginate–acrylamide gels were prepared by modifying a previously published procedure.[43] Sodium alginate (116.7 mg, Thermo Fisher Scientific) and n-isopropylacrylamide (1524.94 mg, Thermo Fisher Scientific) were added to a glass vial containing $(GT)_{15}$-SWCNTs in 1X PBS (1 mg L^{-1}, 20 mL). The vial's contents were dissolved by slow magnetic stirring until visibly homogenous. Ascorbic acid (40 mg, Sigma–Aldrich) was added to the vial, which was then vortexed. Ammonium persulfate (50 mg, Thermo Fisher Scientific) was added to the vial, which was vortexed again and allowed to sit at room temperature for 15 min before being transferred to storage (4 °C).

The resultant solution of 1 mL was transferred to 18 cuvettes, which were covered with parafilm and incubated in a water bath (0.5 h, 40 °C) to gel the alginate–acrylamide copolymer. Fluorescence spectra were acquired from each sample using an NS MiniTracer (1 s exposure). Samples were then divided into three groups ($n = 6$) and topped with 1 mL of either 1X PBS, magnesium chloride ($MgCl_2$, 5 M, Thermo Fisher Scientific), or sodium bicarbonate ($NaHCO_3$, 1 M, Thermo Fisher Scientific).

Fluorescence spectra were again acquired using an NS MiniTracer (1 s exposure) after 1 h of covered incubation in the water bath.

$MgCl_2$ and $NaHCO_3$ Detection in Chitosan Gels: $(GT)_{15}$-SWCNT-containing (1.5 mg L^{-1}) chitosan gels were prepared by modifying a previously published procedure.[44] Deionized water (5955.5 µL) and acetic acid (4.5 µL, Sigma–Aldrich) were added to a glass vial containing chitosan (200 mg, Sigma–Aldrich). The resulting mixture was dissolved by magnetic stirring at 40 °C for at least an hour. To this mixture, glycerol 2-phosphate (3 M, Thermo Fisher Scientific) and $(GT)_{15}$-SWCNTs (3.75 mg L^{-1}) in deionized water (4 mL) were added. The resultant solution was slowly mixed magnetically for at least an hour.

The resultant solution of 1 mL was transferred to each of the nine cuvettes. The samples were covered with parafilm and gelled by incubation in a water bath (40 °C, 1 h). Fluorescence spectra were acquired using an NS MiniTracer (3 s exposure). The samples were then split into three groups and topped with 1 mL of deionized water, $MgCl_2$ (5 M), or $NaHCO_3$ (1 M). Fluorescence spectra were again acquired after 1 h of covered incubation in the water bath. This procedure was repeated for a total of six samples per group.

Methylcellulose-SWCNT Gel Preparation: $(GT)_{15}$-SWCNT-contianing MC gels were prepared by modifying previously published procedure.[42] Briefly, methylcellulose (Sigma–Aldrich) was methacrylated via the esterification of monomeric hydroxyl groups with methacrylic anhydride (Sigma–Aldrich) and then lyophilized for storage. Methacrylated MC was then dissolved in 1X Dulbecco's phosphate buffered saline (Thermo Fisher Scientific) containing $(GT)_{15}$-SWCNTs (1 mg L^{-1}). For sulfonated gels, 2-sulfoethyl methacrylate (PolySciences, Warminster, PA) was added to a final concentration of 5 mM. The resultant polymer-nanotube solution was then split in half to add redox initiators; to one half was added ammonium persulfate (final concentration 10 mM) and to the other was added an equimolar amount of ascorbic acid (Sigma–Aldrich). These solutions were then transferred to a dual barrel syringe fitted with a mixing tip (such that each barrel contained polymers, nanotubes, and one of the redox initiators). Gels were cast by extrusion through the mixing tip.

SWCNT-Gel Fluorescence Stability In Vitro: $(GT)_{15}$-SWCNT-containing 3% sulfonated MC gels were prepared as above and cast in a 1 mL volume into a cuvette ($n = 5$). Fluorescent spectra were obtained via the NS MiniTracer with 638 nm laser excitation 30 min after casting and then the gels within the cuvettes were submerged in 30 mL PBS. At timepoints of 24, 48, 72, 96, and 168 h, the gel was removed and NIR fluorescent spectra were obtained. Data were fit as above and the maximum intensity of the (7,5) chirality plotted individually and as an average ± standard deviation. At the same timepoints, 1 mL of the PBS submersion leachate was removed and fluorescent spectra were obtained with the same parameters as above—the 1 mL was then returned. At the end of 168 h, the entire volume was removed and processed through a 100 kDa molecular weight cutoff filter as above to concentrate any leached SWCNT. The 30 mL volume was concentrated to a volume of 1 mL, which was then measured via the NS MiniTracer as above.

$MgCl_2$ Detection in Methylcellulose Gels: MC gels of 2% and 3% containing $(GT)_{15}$-SWCNTs (1.0 mg L^{-1}) were cast into pre-weighed cuvettes (250-500 mg gel per cuvette). After 30 min, cuvettes were weighed again and gels were topped with 1X PBS as control or $MgCl_2$ (5 M) in 1X PBS and then covered with parafilm. Solution volumes were 1 µL per mg gel. Fluorescence spectra were acquired using an NS MiniTracer (3 s exposure) immediately, every hour for the next 3 h, and every day for the next three days. Samples were stored at 37 °C between measurements.

$NaHCO_3$ Detection in Methylcellulose Gels: MC gels of 2% and 3% containing $(GT)_{15}$-SWCNTs (1.0 mg L^{-1}) were cast into cuvettes (250–500 mg gel per cuvette). After 30 min of incubation, gels were topped with 1X PBS (1 mL) as control or with $NaHCO_3$ (1 M, 1 mL) and then covered with parafilm ($n = 4$). Fluorescence spectra were acquired with an NS MiniTracer (1 s exposure) immediately upon topping, after 1 h, and after two days. Samples were stored at 37 °C between measurements.

$MgCl_2$ Quantification in MC Gels: MC gels of 2% and 3% containing $(GT)_{15}$-SWCNTs (1.0 mg L^{-1}) were cast into pre-weighed cuvettes (250–500 mg gel per cuvette, 20 cuvettes total). After 30 min, cuvettes were weighed. For each MC concentration group (n = 5–6), one cuvette was topped with 1X PBS as a control, and the nine remaining cuvettes were topped with $MgCl_2$ solutions in 1X PBS whose concentrations ranged from 1 M to 3.9 mM, decreasing by half. Solution volumes were 1 µL mg^{-1} gel. Cuvettes were covered with parafilm and stored at 37 °C between measurements. Fluorescence spectra were acquired with an NS MiniTracer (3 s exposure) 1, 2, and 6 days after gels were topped.

$MgCl_2$ and Bovine Serum Albumin Detection in Sulfonated Methylcellulose Gels: MC and MC-SO_3 gels of 2% and 3% containing (GT)15-SWCNTs (1 mg L^{-1}) were cast into 54 pre-weighed cuvettes (250–500 mg gel per cuvette). After 30 min, cuvettes were weighed, and topped with 1X PBS as control, $MgCl_2$ (5 M), or bovine serum albumin (BSA, 600 µM) and then covered with parafilm ($n = 5$–6). Solution volumes were 1 µL mg^{-1} gel. Fluorescence spectra were acquired using an NS MiniTracer (10 s exposure) 1-, 2-, and 6-days post-topping. Samples were stored at 37 °C between measurements. Separately, a set of identical experiments were performed to monitor BSA detection up to two weeks ($n = 7$ for the control group, 6 for the BSA group) with spectra acquired at 1, 2, 3, 4, 7, 8, and 14 days.

Rheological Characterization of Sulfonated Methylcellulose Gels: Rheological measurements were performed as previously described.[42] Characterization was executed at room temperature (n = 3–5) with an AR2000ex Rheometer (TA Instruments, New Castle, DE) using cone and plate geometry (2°, 40 mm). Parameters (0.5% strain, 1 Hz) were selected based on previous work.[42] The gelation time was defined as the delay between initiator mixing and the timepoint when the derivative of G' (the elasticity modulus) was less than 1.

BSA Quantification in Sulfonated Methylcellulose Gels: Each group (solution or gel) consisted of 24 wells with the same concentration of $(GT)_{15}$-SWCNTs; each group tested the response of $(GT)_{15}$-SWCNTs in their respective media to 8 BSA concentrations (including a control) in triplicate.

For the gel group, 3% MC-SO_3 gels containing $(GT)_{15}$-SWCNTs (1 mg L^{-1}) were cast into a 96-well plate (150 ± 50 µL per well, 24 wells). After 30 min, fluorescence spectra were acquired using a ClaIR IR plate-reader, and then these wells were topped with solutions of BSA in 1X PBS (600, 120, 24, 4.8, 0.96, 0.192, 0.0384, and 0 µM; 150 µL; 3 wells per concentration). Fluorescence spectra were acquired immediately after topping, 1, 2, 3, 4, 5, 24, and 48 h thereafter.

For the solution group, solutions of $(GT)_{15}$-SWCNTs in 1X PBS (2 mg L^{-1}) were added to other wells in the same plate (150 µL per well, 21 wells). Fluorescence spectra were acquired before the addition of BSA solutions in 1X PBS (240, 48, 9.6, 1.92, 0.384, 0768, and 0 µM; 150 µL; 3 wells per concentration). Another set of wells was filled with $(GT)_{15}$-SWCNTs (1 mg L^{-1}) and BSA (600 µM) in 1X PBS (300 µL, 3 wells). Fluorescence spectra were acquired immediately, 1, 2, 3, 4, 5, 24, and 48 h thereafter.

Doxorubicin Quantification in Sulfonated Methylcellulose Gels: Each group (solution or gel) consisted of 24 wells with the same concentration of $(GT)_{15}$-SWCNTs; each group tested the response of $(GT)_{15}$-SWCNTs in their respective media to 8 doxorubicin (DOX) concentrations (including a control) in triplicate.

For the gel group, 3% MC-SO_3 gels containing $(GT)_{15}$-SWCNTs (1 mg L^{-1}) were cast into a 96-well plate (150 ± 50 µL per well, 24 wells). After 30 min, fluorescence spectra were acquired using a ClaIR IR plate-reader, and then these wells were topped with solutions of DOX in 1X PBS (1000, 200, 40, 8, 1.6, 0.32, 0.064, and 0 µM; 150 µL; 3 wells per concentration). Fluorescence spectra were acquired immediately after topping, 1, 2, 24, and 48 h thereafter.

For the solution group, solutions of $(GT)_{15}$-SWCNTs in 1X PBS (2 mg L^{-1}) were added to other wells in the same plate (150 µL per well, 21 wells). Fluorescence spectra were acquired before the addition of DOX solutions in 1X PBS (200, 40, 8, 1.6, 0.32, 0.064, and 0 µM; 150 µL; 3 wells per concentration). Because the DOX and $(GT)_{15}$-SWCNTs solutions were equal volumes, the final DOX and SWCNT concentrations of these wells were half those of their respective stock solutions. Another set of wells was filled with $(GT)_{15}$-SWCNTs (1 mg L^{-1}) and DOX (1000 µM) in 1X PBS (300 µL, 3 wells). Fluorescence spectra were acquired immediately, 1, 2, 24, and 48 h thereafter.

Animal Studies: Studies in animals were performed according to the ARRIVE guidelines in 4–6 week old female SKH1-Elite mice (Crl:SKH1-*Hr*^{hr}; Charles River, Wilmington, MA). Animals were housed in separate

cages side-by-side under standard light/dark (12/12) conditions with ad libitum access to food and water. All experiments were approved by the Institutional Animal Care and Use Committee of The City College of New York under protocol #1123 (PI: Williams) Three animals were randomly assigned to receive experimental and control injections (6 total animals), while one animal was used for long-term fluorescence analysis. No animals or time points were excluded from the study analysis. The outcome measures assessed were fluorescence spectra obtained from the IRina NIR-II spectral probe (spectra, center wavelength, and intensity). In comparative injection studies, statistical significance at each time point was determined via a two-tailed *t*-test, and all individual animal data points were reported.

SWCNT-Gel Fluorescence Stability In Vivo: To evaluate the suitability of 3% MC-SO_3 as a SWCNT injection platform, a mouse was injected subcutaneously in the dorsal region with sterile 3% MC-SO_3 containing $(GT)_{15}$-SWCNTs. After 30 min, the mouse was anesthetized with isoflurane, and spectra were acquired using an IRina NIR-II spectral probe. Spectra were again acquired in this fashion after 3, 7, 11, and 61 days.

DOX Detection In Vivo: To evaluate the response of $(GT)_{15}$-SWCNTs in 3% MC-SO_3 to DOX in vivo, ten mice were dorsally injected with the sensor-containing gel using a dual barrel syringe for subcutaneous injection. Fluorescence spectra were acquired using an IRina in vivo NIR-II spectral probe from each mouse under anesthesia 30 min post-injection, after which they were immediately subcutaneously dosed with 10 mg k^{-1}g DOX in 1 mL 1X PBS ($n = 3$ or 1 mL 1X PBS as control ($n = 3$). As mice masses ranged from 18–24 g, doses ranged from 330 to 440 nmol (330–440 µM). Doses were administered in quarters at four locations spaced around the implant site (4 × 250 µL). Spectra were acquired immediately, 10 min, 4, 24, and 48 h after dosing.

Statistical Analyses: Samples were excluded from analysis if contamination or visible air bubbles were observed, as well as when their masses were 25% lower/greater than the average for their groups.

Statistical analyses to determine sensor response significance were performed via two-tailed *t*-tests with unequal variances in MATLAB. Error bars represent the mean ± standard deviation. Where points on graphs represent a difference of a sample group from the control group (e.g., the "shift"), the standard deviation of that difference is calculated as $\sqrt{\text{variance}(control) + \text{variance}(experimental)}$. For intensity comparisons, values were divided by the mean of the control group's intensity (such that the control group's intensity was 100%). Asterisks are used to denote significance thresholds; * for $p < 0.05$, ** for $p < 0.01$, *** for $p < 0.001$, **** for $p < 0.0001$. Sample sizes are in experimental methods subsections.

Supporting Information

Supporting Information is available from the Wiley Online Library or from the author.

Acknowledgements

The authors wish to acknowledge the support of all members of the Williams and Nicoll Labs. This work was supported by NIH NIGMS R35GM142833 (RMW), a CCNY-MSKCC Partnership for Cancer Research Pilot award NIH NCI U54CA132378 and U54CA137788 (RMW and SBN), and a Stand Up to Cancer DISRUPT Pilot award (RMW and SBN).

Conflict of Interest

The authors declare no conflict of interest.

Data Availability Statement

The data that support the findings of this study are available from the corresponding author upon reasonable request.

Keywords

biosensing, carbon nanotubes, doxorubicin, hydrogel, implants, in vivo, methylcellulose, mice, nanosensor, SWCNT

Received: December 28, 2023
Revised: March 30, 2024
Published online:

[1] R. Nissler, J. Ackermann, C. Ma, S. Kruss, *Anal. Chem.* **2022**, *94*, 9941.
[2] R. B. Weisman, S. M. Bachilo, *Nano Lett.* **2003**, *3*, 1235.
[3] G. Hong, A. L. Antaris, H. Dai, *Nat. Biomed. Eng.* **2017**, *1*, 0010.
[4] A. A. Boghossian, J. Zhang, P. W. Barone, N. F. Reuel, J. H. Kim, D. A. Heller, J. H. Ahn, A. J. Hilmer, A. Rwei, J. R. Arkalgud, C. T. Zhang, M. S. Strano, *ChemSusChem* **2011**, *4*, 848.
[5] N. M. Iverson, P. W. Barone, M. Shandell, L. J. Trudel, S. Sen, F. Sen, V. Ivanov, E. Atolia, E. Farias, T. P. McNicholas, N. Reuel, N. M. Parry, G. N. Wogan, M. S. Strano, *Nat. Nanotechnol.* **2013**, *8*, 873.
[6] V. B. Koman, N. A. Bakh, X. Jin, F. T. Nguyen, M. Son, D. Kozawa, M. A. Lee, G. Bisker, J. Dong, M. S. Strano, *Nat. Nanotechnol.* **2022**, *17*, 643.
[7] X. Gong, S. Y. Cho, S. Kuo, B. Ogunlade, K. Tso, D. P. Salem, M. S. Strano, *Anal. Chem.* **2022**, *94*, 16393.
[8] H. Jin, E. S. Jeng, D. A. Heller, P. V. Jena, R. Kirmse, J. Langowski, M. S. Strano, *Macromolecules* **2007**, *40*, 6731.
[9] D. A. Heller, E. S. Jeng, T.-K. Yeung, B. M. Martinez, A. E. Moll, J. B. Gastala, M. S. Strano, *Science* **2006**, *311*, 508.
[10] J. Zhang, A. A. Boghossian, P. W. Barone, A. Rwei, J. H. Kim, D. Lin, D. A. Heller, A. J. Hilmer, N. Nair, N. F. Reuel, M. S. Strano, *J. Am. Chem. Soc.* **2011**, *133*, 567.
[11] V. Zubkovs, H. Wang, N. Schuergers, A. Weninger, A. Glieder, S. Cattaneo, A. A. Boghossian, *Nanoscale Adv* **2022**, *4*, 2420.
[12] J. D. Harvey, R. M. Williams, K. M. Tully, H. A. Baker, Y. Shamay, D. A. Heller, *Nano Lett.* **2019**, *19*, 4343.
[13] M. Son, P. Mehra, F. T. Nguyen, X. Jin, V. B. Koman, X. Gong, M. A. Lee, N. A. Bakh, M. S. Strano, *ACS Nano* **2023**, *17*, 240.
[14] M. C. Ang, N. Dhar, D. T. Khong, T. T. S. Lew, M. Park, S. Sarangapani, J. Cui, A. Dehadrai, G. P. Singh, M. B. Chan-Park, R. Sarojam, M. Strano, *ACS Sens.* **2021**, *6*, 3032.
[15] G. Bisker, N. A. Bakh, M. A. Lee, J. Ahn, M. Park, E. B. O'Connell, N. M. Iverson, M. S. Strano, *ACS Sens.* **2018**, *3*, 367.
[16] M. A. Lee, S. Wang, X. Jin, N. A. Bakh, F. T. Nguyen, J. Dong, K. S. Silmore, X. Gong, C. Pham, K. K. Jones, S. Muthupalani, G. Bisker, M. Son, M. S. Strano, *Adv. Healthcare Mater.* **2020**, *9*, e2000429.
[17] J. Zhang, M. P. Landry, P. W. Barone, J. H. Kim, S. Lin, Z. W. Ulissi, D. Lin, B. Mu, A. A. Boghossian, A. J. Hilmer, A. Rwei, A. C. Hinckley, S. Kruss, M. A. Shandell, N. Nair, S. Blake, F. Sen, S. Sen, R. G. Croy, D. Li, K. Yum, J. H. Ahn, H. Jin, D. A. Heller, J. M. Essigmann, D. Blankschtein, M. S. Strano, *Nat. Nanotechnol.* **2013**, *8*, 959.
[18] S. Kruss, M. P. Landry, E. Vander Ende, B. M. Lima, N. F. Reuel, J. Zhang, J. Nelson, B. Mu, A. Hilmer, M. Strano, *J. Am. Chem. Soc.* **2014**, *136*, 713.
[19] M. Dinarvand, E. Neubert, D. Meyer, G. Selvaggio, F. A. Mann, L. Erpenbeck, S. Kruss, *Nano Lett.* **2019**, *19*, 6604.
[20] P. Kelich, S. Jeong, N. Navarro, J. Adams, X. Sun, H. Zhao, M. P. Landry, L. Vukovic, *ACS Nano* **2022**, *16*, 736.
[21] J. D. Harvey, P. V. Jena, H. A. Baker, G. H. Zerze, R. M. Williams, T. V. Galassi, D. Roxbury, J. Mittal, D. A. Heller, *Nat. Biomed. Eng.* **2017**, *1*, 0041.
[22] G. Bisker, J. Dong, H. D. Park, N. M. Iverson, J. Ahn, J. T. Nelson, M. P. Landry, S. Kruss, M. S. Strano, *Nat. Commun.* **2016**, *7*, 10241.

[23] K. Lee, A. Nojoomi, J. Jeon, C. Y. Lee, K. Yum, *ACS Appl. Nano Mater.* **2018**, *1*, 5327.
[24] M. Antman-Passig, E. Wong, G. R. Frost, C. Cupo, J. Shah, A. Agustinus, Z. Chen, C. Mancinelli, M. Kamel, T. Li, L. A. Jonas, Y. M. Li, D. A. Heller, *ACS Nano* **2022**, *16*, 7269.
[25] X. Jin, M. A. Lee, X. Gong, V. B. Koman, D. J. Lundberg, S. Wang, N. A. Bakh, M. Park, J. I. Dong, D. Kozawa, S.-Y. Cho, M. S. Strano, *ACS Appl. Nano Mater.* **2023**, *6*, 9791.
[26] P. V. Jena, D. Roxbury, T. V. Galassi, L. Akkari, C. P. Horoszko, D. B. Iaea, J. Budhathoki-Uprety, N. Pipalia, A. S. Haka, J. D. Harvey, J. Mittal, F. R. Maxfield, J. A. Joyce, D. A. Heller, *ACS Nano* **2017**, *11*, 10689.
[27] J. Zhang, S. Kruss, A. J. Hilmer, S. Shimizu, Z. Schmois, F. De La Cruz, P. W. Barone, N. F. Reuel, D. A. Heller, M. S. Strano, *Adv. Healthcare Mater.* **2014**, *3*, 412.
[28] R. M. Williams, C. Lee, T. V. Galassi, J. D. Harvey, R. Leicher, M. Sirenko, M. A. Dorso, J. Shah, N. Olvera, F. Dao, D. A. Levine, D. A. Heller, *Sci. Adv.* **2018**, *4*, eaaq1090.
[29] R. M. Williams, C. Lee, D. A. Heller, *ACS Sens.* **2018**, *3*, 1838.
[30] J. Ackermann, J. T. Metternich, S. Herbertz, S. Kruss, *Angew Chem Int Ed Engl* **2022**, *61*, e202112372.
[31] T. V. Galassi, P. V. Jena, J. Shah, G. Ao, E. Molitor, Y. Bram, A. Frankel, J. Park, J. Jessurun, D. S. Ory, A. Haimovitz-Friedman, D. Roxbury, J. Mittal, M. Zheng, R. E. Schwartz, D. A. Heller, *Sci. Transl. Med.* **2018**, *10*, eaar2680.
[32] T. V. Galassi, M. Antman-Passig, Z. Yaari, J. Jessurun, R. E. Schwartz, D. A. Heller, *PLoS One* **2020**, *15*, e0226791.
[33] E. Hofferber, J. Meier, N. Herrera, J. Stapleton, C. Calkins, N. Iverson, *Nanomedicine* **2022**, *40*, 102489.
[34] N. A. Bakh, X. Gong, M. A. Lee, X. Jin, V. B. Koman, M. Park, F. T. Nguyen, M. S. Strano, *Small* **2021**, *17*, e2100540.
[35] M. A. Lee, X. Jin, S. Muthupalani, N. A. Bakh, X. Gong, M. S. Strano, *J Nanobiotechnology* **2023**, *21*, 133.
[36] M. A. Lee, F. T. Nguyen, K. Scott, N. Y. L. Chan, N. A. Bakh, K. K. Jones, C. Pham, P. Garcia-Salinas, D. Garcia-Parraga, A. Fahlman, V. Marco, V. B. Koman, R. J. Oliver, L. W. Hopkins, C. Rubio, R. P. Wilson, M. G. Meekan, C. M. Duarte, M. S. Strano, *ACS Sens.* **2019**, *4*, 32.
[37] S. Correa, A. K. Grosskopf, H. L. Hernandez, D. Chan, A. C. Yu, L. M. Stapleton, E. A. Appel, *Chem. Rev.* **2021**, *121*, 11385.
[38] Z. S. Nishat, T. Hossain, M. N. Islam, H. P. Phan, M. A. Wahab, M. A. Moni, C. Salomon, M. A. Amin, A. A. I. Sina, M. S. A. Hossain, *Small* **2022**, *18*, 2107571.
[39] J. Zhang, Z. Wang, *Catalysts* **2022**, *12*, 1096.
[40] A. Ray, R. Kopelman, *Nanomedicine* **2013**, *8*, 1829.
[41] E. Hofferber, J. Meier, N. Herrera, J. Stapleton, K. Ney, B. Francis, C. Calkins, N. Iverson, *Methods Appl Fluoresc* **2021**, *9*, 025005.
[42] G. T. Gold, D. M. Varma, P. J. Taub, S. B. Nicoll, *Carbohydr. Polym.* **2015**, *134*, 497.
[43] M. J. Chalanqui, S. Pentlavalli, C. McCrudden, P. Chambers, M. Ziminska, N. Dunne, H. O. McCarthy, *Mater Sci Eng C Mater Biol Appl* **2019**, *95*, 409.
[44] H. Qin, J. Wang, T. Wang, X. Gao, Q. Wan, X. Pei, *Front Chem* **2018**, *6*, 565.
[45] Z. Cohen, S. Parveen, R. M. Williams, *ECS J. Solid State Sci. Technol.* **2022**, *11*, 101009.
[46] S. M. Bachilo, M. S. Strano, C. Kittrell, R. H. Hauge, R. E. Smalley, R. B. Weisman, *Science* **2002**, *298*, 2361.
[47] M. Zheng, A. Jagota, E. D. Semke, B. A. Diner, R. S. McLean, S. R. Lustig, R. E. Richardson, N. G. Tassi, *Nat. Mater.* **2003**, *2*, 338.
[48] M. M. Safaee, M. Gravely, A. Lamothe, M. McSweeney, D. Roxbury, *Sci. Rep.* **2019**, *9*, 11926.
[49] D. Roxbury, X. Tu, M. Zheng, A. Jagota, *Langmuir* **2011**, *27*, 8282.
[50] D. Roxbury, P. V. Jena, Y. Shamay, C. P. Horoszko, D. A. Heller, *ACS Nano* **2016**, *10*, 499.
[51] M. Gravely, A. Kindopp, L. Hubert, M. Card, A. Nadeem, C. Miller, D. Roxbury, *ACS Appl. Mater. Interfaces* **2022**, *14*, 19168.
[52] S. A. Varghese, S. M. Rangappa, S. Siengchin, J. Parameswaranpillai, in *Hydrogels Based on Natural Polymers*, Elsevier, Amsterdam, **2020**, pp. 17-47.
[53] M. Card, R. Alejandro, D. Roxbury, *ACS Appl. Mater. Interfaces* **2023**, *15*, 1772.
[54] H. A. Lin, Development and functional evaluation of injectable cellulose-based hydrogels as nucleus pulposus replacements for intervertebral disc repair, New York, **2018**.
[55] P. Nithiyasri, K. Balaji, P. Brindha, M. Parthasarathy, *Nanotechnology* **2012**, *23*, 465603.
[56] F. Tabata, Y. Wada, S. Kawakami, K. Miyaji, *Antioxidants* **2021**, *10*, 503.
[57] J. Budhathoki-Uprety, J. Shah, J. A. Korsen, A. E. Wayne, T. V. Galassi, J. R. Cohen, J. D. Harvey, P. V. Jena, L. V. Ramanathan, E. A. Jaimes, D. A. Heller, *Nat. Commun.* **2019**, *10*, 3605.
[58] B. A. Larsen, P. Deria, J. M. Holt, I. N. Stanton, M. J. Heben, M. J. Therien, J. L. Blackburn, *J. Am. Chem. Soc.* **2012**, *134*, 12485.
[59] L. Zhu, S. Yang, X. Qu, F. Zhu, Y. Liang, F. Liang, Q. Wang, J. Li, Z. Li, Z. Yang, *Polym. Chem.* **2014**, *5*, 5700.
[60] M. Krischke, G. Hempel, S. Völler, N. André, M. D'Incalci, G. Bisogno, W. Köpcke, M. Borowski, R. Herold, A. V. Boddy, *Cancer Chemother. Pharmacol.* **2016**, *78*, 1175.
[61] H. A. Lin, D. M. Varma, W. W. Hom, M. A. Cruz, P. R. Nasser, R. G. Phelps, J. C. Iatridis, S. B. Nicoll, *J. Mech. Behav. Biomed. Mater.* **2019**, *96*, 204.
[62] B. Jachimska, A. Pajor, *Bioelectrochemistry* **2012**, *87*, 138.